Progress In Electromagnetics Research, PIER 75, 85–117, 2007

BIASED MAGNETIC MATERIALS IN RAM APPLICATIONS

J. Ramprecht

Division of Electromagnetic Engineering
School of Electrical Engineering
Royal Institute of Technology
Teknikringen 33, SE-100 44 Stockholm, Sweden

D. Sjöberg

Department of Electrical and Information Technology
Faculty of Engineering
Lund University
Box 118, SE-221 00 Lund, Sweden

Abstract—The magnetization of a ferro- or ferri-magnetic material has been modeled with the Landau-Lifshitz-Gilbert (LLG) equation. In this model demagnetization effects are included. By applying a linearized small signal model of the LLG equation, it was found that the material can be described by an effective permeability and with the aid of a static external biasing field, the material can be switched between a Lorentz-like material and a material that exhibits a magnetic conductivity. Furthermore, the reflection coefficient for normally impinging waves on a PEC covered with a ferro/ferri-magnetic material, biased in the normal direction, is calculated. When the material is switched into the resonance mode, two distinct resonance frequencies in the reflection coefficient were found, one associated with the precession frequency of the magnetization and the other associated with the thickness of the layer. The former of these resonance frequencies can be controlled by the bias field and for a bias field strength close to the saturation magnetization, where the material starts to exhibit a magnetic conductivity, low reflection (around $-20\,\mathrm{dB}$) for a quite large bandwidth (more than two decades) can be achieved.

1. INTRODUCTION

Along with more advanced technology and research progress, highly sophisticated detection systems have been developed. Obviously, especially in military applications, there are occasions where detection is not desirable. As a result, interest has been directed towards methods of reducing detectability, *i.e.*, radar cross section reduction (RCSR).

One of the most important methods to achieve RCSR is by manipulating the shape of the object of interest, so called shaping. This procedure is described, for instance, in [1]. Of course, there are other requirements than those in terms of RCSR that determine the shape of an object(aerodynamic properties etc.), which means that a shape optimized in terms of RCSR may not fulfill additional requirements. Therefore, additional methods for RCSR are needed. One of them, also being mentioned in [1], is using radar absorbing materials (RAM). By reducing the energy reflected back to the radar, radar absorbing materials prevents objects from being detected. The absorption is achieved through dielectric and/or magnetic loss mechanisms that convert electromagnetic energy into heat. Once again, additional requirements than just RCSR are important when designing the RAM. It is often desirable that the RAM is thin, light, durable, inexpensive, insensitive to corrosion and temperature etc. Also, it is important that a RAM absorbs well over a wide range of frequencies. As one might expect, to meet all of these demands in a single design is very difficult and herein lies the challenge for the engineers. One crucial point in the process of designing a RAM is, of course, to understand the loss mechanisms of the materials used and how they should be modeled.

Radar absorbing materials based on dielectric structures and resistive sheets have been in use for quite some time, and are reasonably well understood, including problems involving antenna integration [2, 3]. Two of the oldest and simplest types of such absorbers are the Salisbury screens and the Dallenbach layers.

The Salisbury screen is simply a resistive sheet at a distance of $\lambda/4$ above a metal plate, where λ is the wavelength of the radar wave. At this distance the electric field is maximal, and the energy is absorbed through ohmic losses. Due to the requirement on the wavelength, this absorber is not broadband. The fractional bandwidth at a $-20\,\mathrm{dB}$ reflectivity level is typically about 25% [1, p. 316].

The Dallenbach layer consists of a homogeneous lossy layer backed by a metal plate. The ideal Dallenbach layer, where the material parameters are independent of frequency, with purely dielectric loss has a fractional bandwidth around 20% (at a $-20\,\mathrm{dB}$ reflectivity level)

for a material thickness around $\lambda/4$ at the center frequency [4, p. 621].

These two types of single layer absorbers have difficulties of achieving the bandwidths that are usually required in radar absorbing applications, which can be several decades. By using resistive sheets sandwiched between multiple dielectric layers, the bandwidth can be increased. This design, referred to as the Jaumann absorber, can be viewed as a matching network between the wave impedance of air, $377\,\Omega$, and the short circuit of the metal plate. However, by adding more layers, which have a typical electrical length of $\lambda/4$ at some center frequency, the absorber occupies a lot of space which may not be available. Also, the different dielectric materials often need to have a low permittivity, which is not necessarily compatible with the demand for mechanical strength. Furthermore, the design may be very sensitive to the material parameters in each layer.

Due to their inability to absorb power for low frequencies, materials based on purely dielectric phenomena and electric losses are often considered unsuitable for a broadband absorber design where the available physical space is limited. Therefore it is of interest to investigate whether a material with magnetic losses can be used for the purpose of obtaining thin absorbers that also copes with the broadband requirement. Using magnetic materials as absorbers seems to be an area that is not as well explored as its dielectric counterpart, although practical designs have been in use for a long time. There is no lack of research on magnetism in general, since it is a key component for digital memory technology such as hard disks, and is also important for power transformers. The enormous financial impact of these markets provides a lot of research in magnetism. However, in such applications the engineers are usually more interested in obtaining small losses, whereas engineers working with RCSR are interested in high losses. This research gap is important to close in order to be able to manufacture composite materials with the desired properties.

Magnetism is a difficult subject, much due to the nonlinear nature of many magnetic materials. Therefore, a nonlinear model may be needed which makes the well-posedness of the equations an important and largely unresolved issue [5]. Because of this and since most nonlinear models usually are rather complicated to analyze, one tries to linearize the problem. In the next section we use an isotropic linear model to show that the bandwidth of a Dallenbach layer is improved when adding magnetic losses and in [6] the same conclusion is obtained when a perfectly conducting sphere is coated with a magnetic lossy material. Furthermore, in [7] a finite-difference time-domain method is applied to calculate the radar cross section of cylindrical objects coated with an anisotropic material with electric and/or magnetic losses.

However, these examples use models that are frequency independent, and as such they might not be adequate representations of a realistic magnetic material.

Absorbers consisting of ferrite material have been manufactured and analyzed for some time [3–6]. Recently, composites with ferromagnetic- or ferrite inclusions in a background material have been considered as microwave absorbers [7–11]. These articles treat isotropic materials and composites from an experimental point of view where the main focus rather often is on the manufacturing process, whereas a comparison between numerical methods for composites can be found in [17]. The results reported are based on actual measurements on ferrites or manufactured composites, where the permeability has been measured and from these measurements reflection data from a Dallenbach layer is calculated. The frequencies of interest in these measurements and calculations typically ranges from 0.1–20 GHz. At center frequencies of about 0.2–0.3 GHz, fractional bandwidths (below −20 dB reflectivity level) of 100–140% for a material thicknesses of a few mm is reported [8, 9]. For center frequencies in the range 1–20 GHz the bandwidth is usually smaller. There also exist analyses based on theoretical models of the magnetization [12–14]. Again, isotropic materials are considered and the frequency range is about the same as mentioned above. A multilayer design is also analyzed and an improved bandwidth is reported.

Furthermore, in [21, 22] biased ferrite materials for applications in microwave devices are described. The gyrotropic and non reciprocal property of the biased ferrite is used to construct devices such as gyrators, isolators and circulators. However, for these applications, in difference to radar absorbing applications, small losses are desirable. Finally, commercial products from at least two companies are available on the web[†]. Besides military applications, they also list some interesting civilian applications of magnetic microwaves absorbers, among others RFID: by applying a magnetic surface under the RFID tag, it can be placed directly on an electric conductor without the antenna being shortcircuited by the metal.

In this paper, a theoretical analysis using the Landau-Lifshitz-Gilbert equation to model the dynamics of the magnetization in a biased ferromagnetic/ferrite material is presented. With this model, which includes demagnetization effects, the permeability of the material is obtained and it is found that the material is gyrotropic. The reflection from a perfect electric conductor (PEC) covered with a thin layer (Dallenbach layer) of a magnetic material is studied.

[†] http://www.eccosorb.com
http://www.cfe.com.tw.

Due to the gyrotropic nature of the materialof the material, the polarization of the impinging wave in the analysis have been included. The effects on the reflection of variations in parameters such as saturation magnetization, the damping factor and material thickness are examined. The possibility of controlling the material properties with the aid of an external bias field and how this will affect the absorbing properties of the material is also investigated.

2. MOTIVATING EXAMPLE

At microwave frequencies, which are the frequencies of interest in radar applications, the loss is due to effects on the atomic scale. In this frequency range, the major contribution to the electric losses comes from the finite conductivity of the material, whereas for most magnetic absorbers, the main loss mechanism is magnetization rotation within the domains. However, the engineers are often interested only in the cumulative effects on a macroscopic level and therefore the loss mechanisms are modeled by a phenomenological complex permittivity (ϵ) and permeability (μ), which both may depend on frequency. Furthermore, this model assumes that the material is linear, which often is the case for dielectric materials but usually not for magnetic materials. Nevertheless, a simple linear model is usually a good starting point for obtaining physical insight into the problem.

As a first step in analyzing a magnetic RAM, a simple Dallenbach layer is considered. Hence, the absorber consists of a single slab backed by a PEC where the slab is then assumed to be a homogeneous lossy magnetic material. Not only is the structure of this absorber simple but it is also one of the most common designs for magnetic RAM. To keep things as basic as possible the material is furthermore assumed to be linear, isotropic and frequency independent. The reflection coefficient for normally impinging time-harmonic waves on an isotropic slab of thickness d backed by a PEC is [23, p. 119]

$$r = \frac{r_0 + r_d \mathrm{e}^{\mathrm{i}2k_0 dn}}{1 + r_0 r_d \mathrm{e}^{\mathrm{i}2k_0 dn}} \tag{1}$$

where $k_0 = \omega/c_0$ is the wave number in vacuum (c_0 is the speed of light in vacuum), the PEC is modeled by the reflection coefficient $r_d = -1$, and

$$r_0 = \frac{\eta - 1}{\eta + 1}, \quad \eta = \sqrt{\frac{\mu}{\epsilon}}, \quad n = \sqrt{\epsilon\mu}, \quad \epsilon = \epsilon' + \mathrm{i}\epsilon'' \quad \mu = \mu' + \mathrm{i}\mu'' \tag{2}$$

where ϵ and μ are the relative complex permittivity and permeability, respectively. Introducing real and imaginary parts as

$r_0 = r_0' + \mathrm{i}r_0''$ and $n = n' + \mathrm{i}n''$, we study the expression (1) when $k_0 d$ becomes small to find

$$\begin{aligned} r &= \frac{r_0 - \mathrm{e}^{\mathrm{i}2k_0 dn}}{1 - r_0 \mathrm{e}^{\mathrm{i}2k_0 dn}} \approx \frac{r_0' + \mathrm{i}r_0'' - (1 + \mathrm{i}2k_0 d(n' + \mathrm{i}n''))}{1 - (r_0' + \mathrm{i}r_0'')(1 + \mathrm{i}2k_0 d(n' + \mathrm{i}n''))} \\ &= \frac{r_0' - 1 + 2k_0 dn'' + \mathrm{i}(r_0'' - 2k_0 dn')}{1 - r_0' + r_0'' 2k_0 dn' + r_0' 2k_0 dn'' - \mathrm{i}(r_0'' + r_0' 2k_0 dn' - r_0'' 2k_0 dn'')} \end{aligned} \quad (3)$$

which gives the reflectance

$$\begin{aligned} R &= |r|^2 \\ &\approx \frac{[r_0' - 1 + 2k_0 dn'']^2 + [r_0'' - 2k_0 dn']^2}{[1 - r_0'(1 - 2k_0 dn'') + r_0'' 2k_0 dn']^2 + [r_0''(1 - 2k_0 dn'') + r_0' 2k_0 dn']^2} \end{aligned} \quad (4)$$

First, as $k_0 d$ approaches zero, one would expect that $R \to 1$, *i.e.*, that the reflectance from a PEC is obtained. The same conclusion is also readily obtained from the expression for the reflectance above. Secondly, by examining the expression for the reflection coefficient r_0, one discovers a fundamental difference between electric and magnetic losses, which appears in the imaginary part of r_0. The reflection coefficient $r_0 = (\eta - 1)/(\eta + 1)$ is restricted to the unit circle in the complex plane for all μ and ϵ with $\mu'' > 0$ and $\epsilon'' > 0$. For dominantly electric losses we have $r_0'' < 0$, and dominantly magnetic losses are characterized by $r_0'' > 0$. By dominantly electric losses we mean materials that have the property $\tan\delta_e = \epsilon''/\epsilon' > \tan\delta_m = \mu''/\mu'$, and for dominantly magnetic losses the inequality is reversed. Depending on the sign of r_0'', we get different behaviors of the term $[r_0'' - 2k_0 dn']^2$ in (4) for small $k_0 d$, that is, for thin absorbers. For magnetic losses, $r_0'' > 0$, this term decreases as $k_0 d$ increases, and from Figure 1, it is seen that in order to obtain low reflectance at small frequencies, magnetic losses are superior to electric losses. This conclusion is also reached after studying Figures 8.12–8.14 in [1].

From the above analysis it is seen, in terms of thickness and bandwidth, that low frequency performance of the magnetic material exceeds its electric analogue. The fact that the magnetic field is maximal close to the PEC makes it efficient to place magnetic losses there. Thus, a magnetic layer can be very thin. With the material parameters used in Figure 1 a reflectance level below $-20\,\mathrm{dB}$ is obtained in the interval 4–6 GHz, corresponding to a fractional bandwidth of $(6 - 4)/5 = 40\%$, for a layer just 1 mm thick. This corresponds to a thickness less than 2% of the vacuum wavelength at 5 GHz, which should be compared with the 25% fractional bandwidth obtained with the Salisbury screen, having a thickness of $\lambda/4$ or 25% of

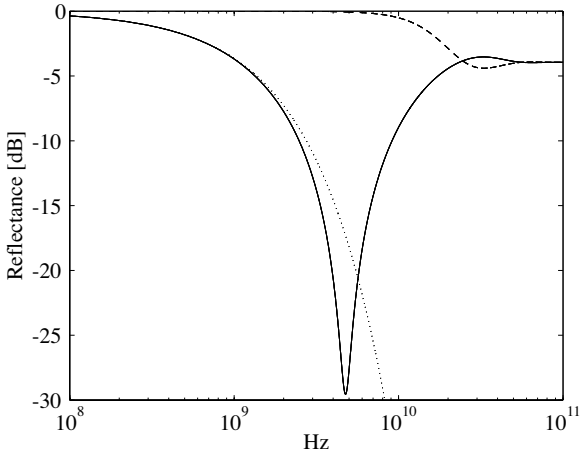

Figure 1. Comparison of the influence of electric and magnetic losses on the reflectance from a 1 mm thick isotropic slab backed by a PEC. The dashed line corresponds to the case $\epsilon = 1 + 10\mathrm{i}$ and $\mu = 1$, and the solid line is $\epsilon = 1$ and $\mu = 1 + 10\mathrm{i}$. The dotted line is an example where $\mu = \epsilon = 1 + 10\mathrm{i}$.

the vacuum wavelength. One should also bear in mind that the results in Figure 1 are based on parameters picked at random and no attempt whatsoever has been made to optimize the design, still a considerable amount of RCSR is achieved. Furthermore, as $k_0 d$ approaches zero and the magnetic layer becomes infinitesimally thin (compared to the wavelength), zero reflection can be obtained [4, p. 616] provided that

$$\omega \mu_0 \mu'' d = \eta_0 \tag{5}$$

$$\mu'' \gg \mu' \tag{6}$$

where η_0 is the vacuum wave impedance.

Provided these requirements are fulfilled for all frequencies, one can, in theory, construct vanishly thin absorbing layers with zero reflection, at all frequencies. This means that μ'' must have a frequency dependence $\sim 1/\omega$. This is sometimes referred to in literature as a magnetic Salisbury screen [4, 1].

In this section we have considered materials with purely electric or magnetic losses in order to get an introductory analysis and comparison of these losses and how they affect the reflectance for a simple Dallenbach layer. However, most magnetic materials available for use in RAM applications generally have both of these loss properties, and are modeled with losses in both permittivity and permeability. Being

able to combine these two parameters gives additional possibilities to design a broadband absorbing material. For instance, if one could find a material that has the property that $\mu = \epsilon$ over a wide range of frequencies, one could in theory devise a broadband RAM for normal incidence. An example of this is shown in Figure 1. With this condition on the material parameters no reflection will occur at the interface between air and the layer (r_0 in (1) is zero), but rather at the interface between the layer and the PEC. Thus, all of the incident wave will be transmitted into the absorber. If the layer is thick enough and has large enough losses, the reflection at the PEC will be negligible. However, in reality few materials can accomplish this.

For the results in Figure 1, μ and ϵ were assumed to be independent of frequency. This is not the case in reality, since for both μ and ϵ the real and imaginary parts are related via the Kramers-Kronig relations [24]. Also, it is seen from (5) that a frequency dependent permeability is required. Thus, in order to find out if it is possible to meet the requirements (5) and (6) for the ideal RAM with magnetic losses and to analyze the absorbing properties of the material more accurately, it is crucial to have a model that includes frequency dependent material parameters.

3. MICROSCOPIC ORIGIN AND MODELING OF MAGNETIC LOSSES

The microscopic origin of magnetism is the spin and orbital momentum of the electron [25, 26], which can be described accurately only by means of quantum mechanics. It is one of few phenomenon on quantum level that is observable by macroscopic means. A nice review of concepts of the physical origin and mechanisms of losses in magnetic materials is presented in [27]. The loss mechanisms are divided into three traditional categories.

Hysteresis losses Due to irreversible flux-change mechanisms, energy is dissipated in the material. These irreversible processes manifest themselves through the famous hysteresis loop for the magnetization curve. The main irreversible mechanism responsible for the magnetic hysteresis loop is domain-wall motion, *i.e.*, the magnetic moments within the domain wall rotate as the wall moves to a new position. There are also instances where uniform rotation of the magnetic moments in the domain (domain-rotation) can be important. However, since domain wall motion experiences a relaxation effect, with a material-dependent frequency that is usually on the order of a few tens to a few hundreds of megahertz, excitation at microwave frequencies

does not cause appreciable domain wall motion in magnetic materials. Thus, hysteresis loss is often negligible in RAM applications.

Eddy-current or dielectric losses An external time-varying magnetic field will cause changes in the orientation of the individual atomic moments in the material, *i.e.*, there are flux-changes. As a consequence, currents are induced in the material, whose associated magnetic fields oppose the domain-wall motion producing the flux change. These currents cause ohmic losses through the finite conductivity.

Residual losses These losses are due to various relaxation processes. The precise interaction mechanisms that are responsible for the magnetic-relaxation processes are far from understood. However, its origin is from magnetic moments interacting in a complicated way with themselves or with the lattice. Among the processes that contribute to the residual losses are the resonance losses, and at high frequencies they often dominate. The resonance phenomena are usually divided into two distinct mechanisms; domain-wall resonance and ferromagnetic resonance.

The losses mentioned above are those attributed to ferro- and ferrimagnetic materials. In contrast to paramagnetic materials where the magnetic moments of the atoms are randomly oriented due to thermal agitation and an external magnetic field is required to align the moments along a specific direction, ferro- and ferrimagnetic materials exhibit domains where the moments are aligned even in the absence of an external field. The magnetization in a domain is therefore given by

$$\boldsymbol{M} = N\boldsymbol{m} \tag{7}$$

where N is the number of magnetic moments per unit volume and $\boldsymbol{m}$ is the magnetic moment of the atoms. Due to the domain structure, the net magnetic moment of a finite sample of a ferromagnetic material is zero because the direction of the magnetization in each domain is random, which means that the magnetization in the different domains cancel each other out. However, when a sufficiently strong external dc magnetic field is applied and for an appropriate shape of the sample, all the magnetic dipoles are aligned parallel to each other and the sample behaves like a single domain. When this state is reached the sample is said to be magnetically saturated and the net magnetization, called saturation magnetization, is then given by (7). It should also be mentioned that the spontaneous magnetization in the domain vanishes above a critical temperature T_{c} called the Curie temperature. Above T_{c} the material behaves like a paramagnetic

material. In Table 1 saturation magnetization and Curie temperature for different substances are presented.

Table 1. Saturation magnetization, M_s, and Curie temperature for ferromagnetic crystals [25].

Substance	M_s ($\cdot 10^5$ **A/m**)		**Curie temp.(in K)**
	Room temp.	0 K	T_c
Fe	17.07	17.40	1043
Co	14.00	14.46	1388
Ni	4.85	5.10	627
Gd	-	20.60	292
Dy	-	29.20	88
MnAs	6.70	8.70	318
CrO_2	5.15	-	386
$NiOFe_2O_3$	2.70	-	858
$MgOFe_2O_3$	1.10	-	713

It can be shown [28, 22, 21, 29] that the dynamics of the magnetization in a domain, when interacting with a magnetic field is given by

$$\frac{\partial \boldsymbol{M}}{\partial t} = -\gamma \mu_0 \boldsymbol{M} \times \boldsymbol{H} \tag{8}$$

where

$$\gamma = ge/2m_e = 1.759 \times 10^{11} \mathrm{C/kg} \tag{9}$$

is the gyromagnetic ratio for the material, m_e and e represent the mass and charge of the electron and the g-factor (spectroscopic splitting factor) is $\cong 2$ for most ferro- and ferrimagnetic materials used in microwave applications. From this equation it is found that if $\boldsymbol{H}$ is a static field $\hat{\boldsymbol{n}} H_0$, where $\hat{\boldsymbol{n}}$ is an arbitrary unit vector, then the magnetization $\boldsymbol{M}$ precesses about the $\hat{\boldsymbol{n}}$ axis with an angular frequency

$$\omega_0 = \gamma \mu_0 H_0 \tag{10}$$

where H_0 is the magnitude of the dc magnetic field, the biasing field. Hence, equation (8) describes a uniform precession of the magnetic moments in the domain, about the biasing field. Furthermore, if a small time harmonic magnetic field H_1 with frequency equal to the

precession frequency of the magnetization is superimposed on H_0, then it can be shown [29] that, in a small signal approximation regime, the amplitude of the magnetization tends to grow and energy is transferred from the magnetic field to the material in an efficient way, *i.e.*, we have a resonance condition. In fact, with this approximation the precessional amplitude grows to infinity in the direction perpendicular to the static $\boldsymbol{H}$-field. However, due to the loss mechanisms described above, such singularities are damped out in a real magnetic material, and the precession is finite. Since these loss mechanisms are many and some of them complicated and not very well understood, they are modeled by a phenomenological damping term that is added to (8) in the following way

$$\frac{\partial \boldsymbol{M}}{\partial t} = -\gamma\mu_0 \boldsymbol{M} \times \boldsymbol{H} - \frac{\Lambda}{|\boldsymbol{M}|^2} \boldsymbol{M} \times (\boldsymbol{M} \times \boldsymbol{H}) \tag{11}$$

where Λ has the dimension $[\text{time}]^{-1}$ and is a (positive) phenomenological parameter that represents all the losses. Due to its dimension, Λ is called the relaxation frequency. This damping term, first proposed by Landau and Lifshitz [30] in 1935, is in effect a resistive torque pulling back the magnetization toward the $\boldsymbol{H}$-field and thus preventing the precession to become infinite.

Another form of the damping term was proposed by T. L. Gilbert [31]. He reasoned that the damping term should depend on the time derivative of the magnetization and suggested the model

$$\frac{\partial \boldsymbol{M}}{\partial t} = -\gamma\mu_0 \boldsymbol{M} \times \boldsymbol{H} + \alpha \frac{\boldsymbol{M}}{|\boldsymbol{M}|} \times \frac{\partial \boldsymbol{M}}{\partial t} \tag{12}$$

in which α is a dimensionless constant, called the damping factor. This equation is often referred to as the Landau-Lifshitz-Gilbert equation(LLG). The damping factor can be found from the resonance line halfwidth measurements [28, 22, 29] and it seems that its largest value is of the order $\alpha \approx 0.1$, although some values as large as 0.4 or even 0.92 can be found in the literature [20, 32] .

The LLG-equation (12) and Landau-Lifshitz equation (11) are very similar in mathematical structure. In fact, the LLG-equation can with a few straightforward manipulations be transformed into a Landau-Lifshitz equation. However, there is a substantial difference between the two equations. In the limit when the damping goes to infinity, $\lambda \to \infty$ in (11) and $\alpha \to \infty$ in (12), the LL-equation and LLG-equation give respectively:

$$\frac{\partial \boldsymbol{M}}{\partial t} \to \infty, \frac{\partial \boldsymbol{M}}{\partial t} \to 0 \tag{13}$$

The result, increased damping accompanied by faster motion obtained from the LL-equation is somewhat counterintuitive and physically implausible. Because of this behavior, it is argued [31, 33, 34] that the LLG model is to prefer.

From the LL- and LLG equation it is seen that the magnitude of the magnetization is preserved. Since the right hand side is orthogonal to $\boldsymbol{M}$, we have

$$\boldsymbol{M} \cdot \frac{\partial \boldsymbol{M}}{\partial t} = \frac{1}{2} \frac{\partial |\boldsymbol{M}|^2}{\partial t} = 0 \quad \Rightarrow \quad |\boldsymbol{M}| = M_{\mathrm{s}} \tag{14}$$

where the constant M_{s} is the saturation magnetization. Hence, only the orientation of the magnetization can change, not the magnitude.

Equations (11) and (12) do not take into account several interactions present in real ferro- and ferrimagnetic materials. In order to incorporate these interactions, the magnetic field, $\boldsymbol{H}$, is replaced by an effective magnetic field, $\boldsymbol{H}_{\mathrm{eff}}$, that includes other torque-producing contributions besides the external magnetic field. The effective magnetic field can be modeled in the following way [29, 31, 35]

$$\boldsymbol{H}_{\mathrm{eff}} = \boldsymbol{H} + \boldsymbol{H}_{\mathrm{an}} + \boldsymbol{H}_{\mathrm{ex}} + \boldsymbol{H}_{\mathrm{me}} \tag{15}$$

where the different terms are: 1) the classical magnetic field, $\boldsymbol{H}$, appearing in Maxwell's equations 2) the crystal anisotropy field $\boldsymbol{H}_{\mathrm{an}} = -\mathbf{N}_{\mathrm{c}} \cdot \boldsymbol{M}$ due to magnetocrystalline anisotropy of a ferro- or ferrimagnetic material, 3) the exchange field $\boldsymbol{H}_{\mathrm{ex}} = \lambda_{\mathrm{ex}} \nabla^2 \boldsymbol{M}$ due to non-uniform exchange interaction of the precessing spins 4) the magnetoelastic field $\boldsymbol{H}_{\mathrm{me}}$ due to interaction between the magnetization and the mechanical strain of the lattice. The anisotropy tensor $\mathbf{N}_{\mathrm{c}}$ is assumed to be known, as well as the exchange constant λ_{ex}. For a uniaxial crystal with axis $\hat{\boldsymbol{n}}$, the anisotropy tensor becomes $\mathbf{N}_{\mathrm{c}} = N_{\mathrm{c}} \hat{\boldsymbol{n}} \hat{\boldsymbol{n}}$. The case $N_{\mathrm{c}} < 0$ is termed easy axis, and the case $N_{\mathrm{c}} > 0$ is termed easy plane. Due to [36, eq. (2.21)], N_{c} can be computed as $N_{\mathrm{c}} = -2K_1/\left(\mu_0 M_{\mathrm{s}}^2\right)$, where K_1 is the uniaxial magnetocrystalline anisotropy constant as given in [36, p. 137]. The exchange length of the material, defined by $l_{\mathrm{ex}} = \sqrt{\lambda_{\mathrm{ex}}}$, is also given for different materials in [36, p. 137]. From this, it is seen that the exchange length is in the order of $3 - 10$nm.

4. SMALL AMPLITUDE APPROXIMATION

In RAM applications it is reasonable to assume that the magnetic field $\boldsymbol{H}$ can be divided into two parts, $\boldsymbol{H} = \boldsymbol{H}_0 + \boldsymbol{H}_1$. In this decomposition

$\boldsymbol{H}_0$ is a strong static field and $\boldsymbol{H}_1$ is a weak, time-harmonic field due to an incoming radar wave, *i.e.*, $|\boldsymbol{H}_1| \ll |\boldsymbol{H}_0|$. Therefore it is convenient to represent the magnetization by a static part $\boldsymbol{M}_0$ and a time-harmonic part $\boldsymbol{M}_1$ as $\boldsymbol{M} = \boldsymbol{M}_0 + \boldsymbol{M}_1$, where $|\boldsymbol{M}_1| \ll |\boldsymbol{M}_0|$. The static field $\boldsymbol{M}_0$ is the magnetization induced by the static $\boldsymbol{H}_0$-field whereas $\boldsymbol{M}_1$ is the magnetization induced by the small perturbation $\boldsymbol{H}_1$. The static part of the magnetization satisfies $|\boldsymbol{M}_0| = M_{\mathrm{s}}$, and we can represent the zeroth order magnetization by

$$\boldsymbol{M}_0 = M_{\mathrm{s}}\boldsymbol{m}_0, \qquad |\boldsymbol{m}_0| = 1 \tag{16}$$

If we ignore the exchange field and the magnetoelastic fields in (15), the effective field is

$$\boldsymbol{H}_{\mathrm{eff}} = \boldsymbol{H}_0 - \mathbf{N}_{\mathrm{c}}\boldsymbol{M}_0 + \boldsymbol{H}_1 - \mathbf{N}_{\mathrm{c}}\boldsymbol{M}_1 = \boldsymbol{H}_{\mathrm{eff},0} + \boldsymbol{H}_{\mathrm{eff},1} \tag{17}$$

where $\boldsymbol{H}_{\mathrm{eff},0} = \boldsymbol{H}_0 - \mathbf{N}_{\mathrm{c}}\boldsymbol{M}_0$ is the static effective field and $\boldsymbol{H}_{\mathrm{eff},1} = \boldsymbol{H}_1 - \mathbf{N}_{\mathrm{c}}\boldsymbol{M}_1$ is the time varying effective field.

For the special case of a spheroidal particle immersed in a homogeneous external bias field $\boldsymbol{H}_0^{\mathrm{e}}$, the particle is uniformly magnetized, and the total classical field within the particle can be shown to be

$$\boldsymbol{H}_0 = \boldsymbol{H}_0^{\mathrm{e}} - \mathbf{N}_{\mathrm{d}}\boldsymbol{M}_0 \tag{18}$$

where $\mathbf{N}_{\mathrm{d}}$ is the demagnetization tensor for the particle and in Table 2 some demagnetization tensors are shown for different extremes of spheroidal particles [37]. Hence, the static part of the effective field becomes

$$\boldsymbol{H}_{\mathrm{eff},0} = \boldsymbol{H}_0^{\mathrm{e}} - (\mathbf{N}_{\mathrm{d}} + \mathbf{N}_{\mathrm{c}})\,\boldsymbol{M}_0 = \boldsymbol{H}_0^{\mathrm{e}} - \mathbf{N}\boldsymbol{M}_0 \tag{19}$$

and the time varying effective field is

$$\boldsymbol{H}_{\mathrm{eff},1} = \boldsymbol{H}_1 - \mathbf{N}_{\mathrm{c}}\boldsymbol{M}_1 \tag{20}$$

At this point we choose to neglect the anisotropy of the crystal. This can be justified for certain ferromagnetic uniaxial crystals where the value of N_{c} is of the order 10^{-2}, *i.e.*, a rather small number. This leaves us with the following expression for the effective field

$$\boldsymbol{H}_{\mathrm{eff}} = \boldsymbol{H}_0^{\mathrm{e}} - \mathbf{N}_{\mathrm{d}}\boldsymbol{M}_0 + \boldsymbol{H}_1 = \boldsymbol{H}_0 + \boldsymbol{H}_1 \tag{21}$$

Substituting this effective field into the LLG equation (12) results in

$$\frac{\partial(\boldsymbol{M}_0 + \boldsymbol{M}_1)}{\partial t} = -\gamma\mu_0\left[(\boldsymbol{M}_0 + \boldsymbol{M}_1) \times (\boldsymbol{H}_0 + \boldsymbol{H}_1)\right] + \alpha\frac{(\boldsymbol{M}_0 + \boldsymbol{M}_1)}{M_{\mathrm{s}}} \times \frac{\partial(\boldsymbol{M}_0 + \boldsymbol{M}_1)}{\partial t} \tag{22}$$

Table 2. Demagnetization tensors for different shapes.

Shape	$\mathbf{N}_\mathrm{d}$
Sphere	$\begin{pmatrix} 1/3 & 0 & 0 \\ 0 & 1/3 & 0 \\ 0 & 0 & 1/3 \end{pmatrix}$
Thin plate (normal in z-direction)	$\begin{pmatrix} 0 & 0 & 0 \\ 0 & 0 & 0 \\ 0 & 0 & 1 \end{pmatrix}$
Thin rod (in z-direction)	$\begin{pmatrix} 1/2 & 0 & 0 \\ 0 & 1/2 & 0 \\ 0 & 0 & 0 \end{pmatrix}$

Since $\boldsymbol{M}_0$ corresponds to a static solution, *i.e.*, $\frac{\partial \boldsymbol{M}_0}{\partial t} = 0$, the zeroth order term gives

$$\begin{aligned} \boldsymbol{M}_0 \times \boldsymbol{H}_0 &= \boldsymbol{M}_0 \times (\boldsymbol{H}_0^\mathrm{e} - \mathbf{N}_\mathrm{d}\boldsymbol{M}_0) = 0 && (23) \\ &\Rightarrow \boldsymbol{H}_0^\mathrm{e} - \mathbf{N}_\mathrm{d}\boldsymbol{M}_0 = \beta \boldsymbol{M}_0 && (24) \\ &\Rightarrow \boldsymbol{m}_0 = (\beta \mathbf{I} + \mathbf{N}_\mathrm{d})^{-1} \boldsymbol{H}_0^\mathrm{e}/M_\mathrm{s} && (25) \end{aligned}$$

where β is a constant and is determined from the condition $|\boldsymbol{m}_0| = 1$. For the special case of a spherical particle, we have $\mathbf{N}_\mathrm{d} = \mathbf{I}/3$, and $\beta = \pm|\boldsymbol{H}_0^\mathrm{e}|/M_\mathrm{s} - 1/3$. In the case of a bias field in the normal direction of a thin plate we have $\beta = \pm|\boldsymbol{H}_0^\mathrm{e}|/M_\mathrm{s} - 1$ [‡]. From this it is seen that if the bias field is in the normal direction of the thin plate, then $\boldsymbol{M}_0$ will also be in this direction.

First order terms give (assuming H_1 has an $\mathrm{e}^{-\mathrm{i}\omega t}$ time dependence so that $\boldsymbol{M}_1(\boldsymbol{r}, t) \approx \boldsymbol{M}_1(\boldsymbol{r})\,\mathrm{e}^{-\mathrm{i}\omega t}$ and $\frac{\partial \boldsymbol{M}_1}{\partial t} = -\mathrm{i}\omega \boldsymbol{M}_1$)

$$-\mathrm{i}\omega \boldsymbol{M}_1 = -\gamma\mu_0 \left[\boldsymbol{M}_0 \times \boldsymbol{H}_1 + \boldsymbol{M}_1 \times (\boldsymbol{H}_0^\mathrm{e} - \mathbf{N}_\mathrm{d}\boldsymbol{M}_0)\right] - \alpha \frac{\boldsymbol{M}_0}{M_\mathrm{s}} \times \mathrm{i}\omega \boldsymbol{M}_1 \tag{26}$$

Collecting all terms containing $\boldsymbol{M}_1$ on the left hand side implies

$$\left[-\mathrm{i}\omega \mathbf{I} - \gamma\mu_0 (\boldsymbol{H}_0^\mathrm{e} - \mathbf{N}_\mathrm{d}\boldsymbol{M}_0) \times \mathbf{I} + \mathrm{i}\omega\alpha \frac{\boldsymbol{M}_0}{M_\mathrm{s}} \times \mathbf{I}\right] \boldsymbol{M}_1 = -\gamma\mu_0 \boldsymbol{M}_0 \times \boldsymbol{H}_1 \tag{27}$$

[‡] The minus signs in the solutions of β corresponds to the magnetization being antiparallel to the applied external field, which we consider an unstable solution. Thus, we deal only with the plus sign from now on.

where $\mathbf{I}$ is the identity matrix.

Since we have $\beta \boldsymbol{M}_0 = \boldsymbol{H}_0^{\mathrm{e}} - \mathbf{N}_{\mathrm{d}} \boldsymbol{M}_0$ from before, this equation can also be written

$$\left[-\mathrm{i}\omega \mathbf{I} - (\gamma \mu_0 \beta M_{\mathrm{s}} - \mathrm{i}\omega\alpha) \frac{\boldsymbol{M}_0}{M_{\mathrm{s}}} \times \mathbf{I} \right] \boldsymbol{M}_1 = -\gamma \mu_0 \boldsymbol{M}_0 \times \boldsymbol{H}_1 \tag{28}$$

Introducing

$$\omega_{\mathrm{m}} = \gamma \mu_0 M_{\mathrm{s}} \quad \text{andusing} \quad \boldsymbol{m}_0 = \frac{\boldsymbol{M}_0}{M_{\mathrm{s}}} \tag{29}$$

one obtains

$$\left[-\mathrm{i}\omega \mathbf{I} - (\omega_{\mathrm{m}} \beta - \mathrm{i}\omega\alpha) \boldsymbol{m}_0 \times \mathbf{I} \right] \boldsymbol{M}_1 = -\omega_{\mathrm{m}} \boldsymbol{m}_0 \times \boldsymbol{H}_1 \tag{30}$$

From this equation it is then seen that $\boldsymbol{m}_0 \cdot \boldsymbol{M}_1 = 0$, which means we only have to consider components orthogonal to $\boldsymbol{m}_0$. The matrix on the left hand side is then (where the cross product $\boldsymbol{m}_0 \times \mathbf{I}$ is represented by the matrix $\left(\begin{smallmatrix} 0 & -1 \\ 1 & 0 \end{smallmatrix}\right)$)

$$\begin{aligned} -\mathrm{i}\omega \mathbf{I} - (\omega_{\mathrm{m}} \beta - \mathrm{i}\omega\alpha) \boldsymbol{m}_0 \times \mathbf{I} &= -\mathrm{i}\omega \begin{pmatrix} 1 & 0 \\ 0 & 1 \end{pmatrix} - (\omega_{\mathrm{m}} \beta - \mathrm{i}\omega\alpha) \begin{pmatrix} 0 & -1 \\ 1 & 0 \end{pmatrix} \\ &= \begin{pmatrix} -\mathrm{i}\omega & \omega_{\mathrm{m}} \beta - \mathrm{i}\omega\alpha \\ -\omega_{\mathrm{m}} \beta + \mathrm{i}\omega\alpha & -\mathrm{i}\omega \end{pmatrix} \end{aligned} \tag{31}$$

The equation is then on the form

$$\begin{pmatrix} a_{11} & a_{12} \\ a_{21} & a_{22} \end{pmatrix} \begin{pmatrix} M_{1,1} \\ M_{1,2} \end{pmatrix} = -\omega_{\mathrm{m}} \begin{pmatrix} 0 & -1 \\ 1 & 0 \end{pmatrix} \begin{pmatrix} H_{1,1} \\ H_{1,2} \end{pmatrix} \tag{32}$$

with the explicit solution

$$\begin{aligned} \begin{pmatrix} M_{1,1} \\ M_{1,2} \end{pmatrix} &= -\frac{\omega_{\mathrm{m}}}{a_{11}a_{22} - a_{12}a_{21}} \begin{pmatrix} a_{22} & -a_{12} \\ -a_{21} & a_{11} \end{pmatrix} \begin{pmatrix} 0 & -1 \\ 1 & 0 \end{pmatrix} \begin{pmatrix} H_{1,1} \\ H_{1,2} \end{pmatrix} \\ &= -\frac{\omega_{\mathrm{m}}}{a_{11}a_{22} - a_{12}a_{21}} \begin{pmatrix} -a_{12} & -a_{22} \\ a_{11} & a_{21} \end{pmatrix} \begin{pmatrix} H_{1,1} \\ H_{1,2} \end{pmatrix} \end{aligned} \tag{33}$$

The small signal susceptibility is defined from the relation $\boldsymbol{M}_1 = \boldsymbol{\chi} \boldsymbol{H}_1$ and since the components parallel to $\boldsymbol{m}_0$ were shown to be zero, we have

$$\boldsymbol{\chi} = \frac{1}{(\beta - \mathrm{i}\alpha\omega/\omega_{\mathrm{m}})^2 - (\omega/\omega_{\mathrm{m}})^2} \begin{pmatrix} \beta - \mathrm{i}\alpha\omega/\omega_{\mathrm{m}} & -\mathrm{i}\omega/\omega_{\mathrm{m}} & 0 \\ \mathrm{i}\omega/\omega_{\mathrm{m}} & \beta - \mathrm{i}\alpha\omega/\omega_{\mathrm{m}} & 0 \\ 0 & 0 & 0 \end{pmatrix} \tag{34}$$

The permeability tensor $\boldsymbol{\mu}$ is defined through $\boldsymbol{B}_1 = \mu_0(\boldsymbol{M}_1 + \boldsymbol{H}_1) = \mu_0(\boldsymbol{\chi} + \mathbf{I})\,\boldsymbol{H}_1 = \mu_0\boldsymbol{\mu}\boldsymbol{H}_1$, and in this case it has the form of a gyrotropic tensor

$$\boldsymbol{\mu} = \begin{pmatrix} \mu & \mathrm{i}\mu_g & 0 \\ -\mathrm{i}\mu_g & \mu & 0 \\ 0 & 0 & \mu_z \end{pmatrix} \tag{35}$$

where

$$\mu(\omega) = 1 + \frac{\beta - \mathrm{i}\alpha\omega/\omega_\mathrm{m}}{(\beta - \mathrm{i}\alpha\omega/\omega_\mathrm{m})^2 - (\omega/\omega_\mathrm{m})^2} \tag{36}$$

$$\mu_g(\omega) = -\frac{\omega/\omega_\mathrm{m}}{(\beta - \mathrm{i}\alpha\omega/\omega_\mathrm{m})^2 - (\omega/\omega_\mathrm{m})^2} \tag{37}$$

$$\mu_z(\omega) = 1 \tag{38}$$

The losses are connected to the anti-hermitian part of the permeability tensor. In analogy with the electric conductivity, a magnetic conductivity tensor can be defined as $\boldsymbol{\sigma}_\mathrm{m} = -\mathrm{i}\omega\mu_0\left(\boldsymbol{\mu} - \boldsymbol{\mu}^\dagger\right)/2$ [38], although it has units of $[\boldsymbol{\sigma}_\mathbf{m}] = \Omega/\mathrm{m}$ and not S/m as in the electric case. With the permeability tensor described above and after some algebra, this is found to be (neglecting components parallel to $\boldsymbol{m}_0$ since they are zero)

$$\boldsymbol{\sigma}_\mathrm{m} = -\mathrm{i}\omega\mu_0\frac{\boldsymbol{\mu} - \boldsymbol{\mu}^\dagger}{2} = \frac{\alpha\mu_0\omega_\mathrm{m}(\omega/\omega_\mathrm{m})^2}{\left(\beta^2 - (1+\alpha^2)(\omega/\omega_\mathrm{m})^2\right)^2 + 4\alpha^2(\omega/\omega_\mathrm{m})^2\,\beta^2} \cdot \begin{pmatrix} \beta^2 + \left(1+\alpha^2\right)(\omega/\omega_\mathrm{m})^2 & -2\mathrm{i}\beta\omega/\omega_\mathrm{m} \\ 2\mathrm{i}\beta\omega/\omega_\mathrm{m} & \beta^2 + \left(1+\alpha^2\right)(\omega/\omega_\mathrm{m})^2 \end{pmatrix} \tag{39}$$

Since β depend on the bias field, $\boldsymbol{H}_0^\mathrm{e}$ (for instance, $\beta = |\boldsymbol{H}_0^\mathrm{e}|/M_\mathrm{s} - 1$ for the flat plate with bias field in the normal direction), we have the possibility to control the value of β with the aid of this bias field. For the special case of $\beta = 0$, the magnetic conductivity is independent of frequency

$$\boldsymbol{\sigma}_\mathrm{m} \overset{\beta=0}{=} \mu_0\omega_\mathrm{m}\frac{\alpha}{1+\alpha^2}\mathbf{I} \tag{40}$$

Thus, in this particular case($\beta = 0$), $\boldsymbol{\sigma}_\mathrm{m}$ can be used to represent a magnetic conductivity tensor, which is independent of frequency. From the above analysis it is seen that with the aid of $\boldsymbol{H}_0^\mathrm{e}$, it is possible (at least in theory) to change the character of the material. The material can be switched between a material that behaves like a Lorentz material with a resonance frequency, and a material that exhibits a magnetic conductivity tensor.

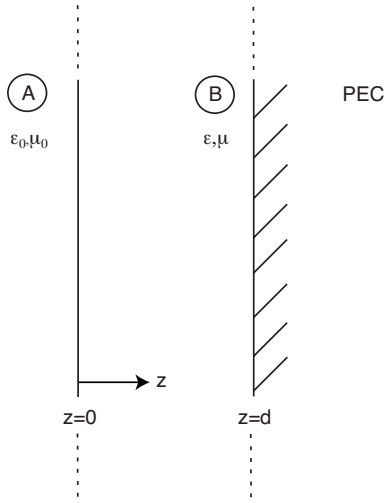

Figure 2. Slab of a ferromagnetic material with thickness d on a PEC.

5. REFLECTION FROM PEC COATED WITH FERROMAGNETIC MATERIAL

In this section the reflection coefficient for normally impinging waves on a Dallenbach layer with material parameters given by (35) and an isotropic permittivity, $\epsilon\mathbf{I}$, is calculated. The situation is depicted in Figure 2. It is assumed that the static external biasing field $\boldsymbol{H}_0^{\mathrm{e}}$ is in the $\hat{\boldsymbol{z}}$-direction and that the impinging wave is propagating along this direction. This impinging wave is then represented by an impressed time-harmonic field, and the field inside the material is the field $\boldsymbol{H}_1$ that is used in (17).

Materials represented by permittivity- and permeability tensors on the form like (35) are referred to as gyrotropic media. The wave propagation along the $\hat{\boldsymbol{z}}$-direction in gyrotropic media is well known and the so called eigenmodes for the material, that represents the field $\boldsymbol{H}_1$, are given by (see [21, 22] for detailed discussion)

$$\begin{cases} \boldsymbol{H}^+ = H^+(\hat{\boldsymbol{x}} - \mathrm{i}\hat{\boldsymbol{y}})\,\mathrm{e}^{\pm \mathrm{i}k_+ z} \\ \boldsymbol{H}^- = H^-(\hat{\boldsymbol{x}} + \mathrm{i}\hat{\boldsymbol{y}})\,\mathrm{e}^{\pm \mathrm{i}k_- z} \end{cases} \tag{41}$$

where $k_\pm = \frac{\omega}{c_0}(\epsilon(\mu \pm \mu_g))^{\frac{1}{2}}$ and the $\boldsymbol{E}$- and $\boldsymbol{H}$-fields are related to each other in the following way

$$\begin{cases} \boldsymbol{E}^+ = \mp\eta_0 Z^+ \hat{\boldsymbol{z}} \times \boldsymbol{H}^+ \\ \boldsymbol{E}^- = \mp\eta_0 Z^- \hat{\boldsymbol{z}} \times \boldsymbol{H}^- \end{cases} \tag{42}$$

where the minus (plus) sign corresponds to propagation in the positive (negative) $\hat{\boldsymbol{z}}$-direction and $Z^{\pm} = \left(\frac{1}{\epsilon}(\mu \pm \mu_g)\right)^{\frac{1}{2}}$.

In the vacuum region we are free to choose the polarization of the fields at will. However, since the polarization in the material is restricted to the eigenmodes which in this case are circularly polarized, it is convenient to represent the polarization in the vacuum region in this polarization state as well. Setting up the in- and outgoing eigenmodes in the different regions then yields:

Region A (vacuum region):

$$\begin{aligned} \boldsymbol{H}_1 &= \boldsymbol{H}_i e^{\mathrm{i}k_1 z} + \boldsymbol{H}_r e^{-\mathrm{i}k_1 z} \\ &= \left[H_i^+(\hat{\boldsymbol{x}} - \mathrm{i}\hat{\boldsymbol{y}}) + H_i^-(\hat{\boldsymbol{x}} + \mathrm{i}\hat{\boldsymbol{y}})\right] e^{\mathrm{i}k_1 z} \\ &\quad + \left[H_r^+(\hat{\boldsymbol{x}} - \mathrm{i}\hat{\boldsymbol{y}}) + H_r^-(\hat{\boldsymbol{x}} + \mathrm{i}\hat{\boldsymbol{y}})\right] e^{-\mathrm{i}k_1 z} \qquad (43) \\ \boldsymbol{E}_1 &= -\eta_0 \hat{\boldsymbol{z}} \times \boldsymbol{H}_i e^{\mathrm{i}k_1 z} + \eta_0 \hat{\boldsymbol{z}} \times \boldsymbol{H}_r e^{-\mathrm{i}k_1 z} \qquad (44) \end{aligned}$$

Region B (material region):

$$\begin{aligned} \boldsymbol{H}_1 &= \left[H_+^+ e^{\mathrm{i}k_+ z} + H_-^+ e^{-\mathrm{i}k_+ z}\right](\hat{\boldsymbol{x}} - \mathrm{i}\hat{\boldsymbol{y}}) \\ &\quad + \left[H_+^- e^{\mathrm{i}k_- z} + H_-^- e^{-\mathrm{i}k_- z}\right](\hat{\boldsymbol{x}} + \mathrm{i}\hat{\boldsymbol{y}}) \qquad (45) \\ \boldsymbol{E}_1 &= \eta_0 Z^+ \hat{\boldsymbol{z}} \times (\hat{\boldsymbol{x}} - \mathrm{i}\hat{\boldsymbol{y}}) \left[-H_+^+ e^{\mathrm{i}k_+ z} + H_-^+ e^{-\mathrm{i}k_+ z}\right] \\ &\quad + \eta_0 Z^- \hat{\boldsymbol{z}} \times (\hat{\boldsymbol{x}} + \mathrm{i}\hat{\boldsymbol{y}}) \left[-H_+^- e^{\mathrm{i}k_- z} + H_-^- e^{-\mathrm{i}k_- z}\right] \qquad (46) \end{aligned}$$

where $k_1 = \omega/c_0$ and $\eta_0 = \sqrt{\frac{\mu_0}{\epsilon_0}}$.

The total field in both regions can be represented by the sum of two orthogonal modes (right- and left-hand circularly polarized modes) that do not couple into each other. This means that one can separate the two modes and analyze the reflection coefficient for each mode separately. In fact, this will be exactly analogous to the case discussed in Section 2 for an isotropic layer. Hence, the reflection coefficient for each mode will take the form (1) or written in matrix form for both modes

$$\begin{pmatrix} E_r^+ \\ E_r^- \end{pmatrix} = \begin{pmatrix} r_+ & 0 \\ 0 & r_- \end{pmatrix} \begin{pmatrix} E_i^+ \\ E_i^- \end{pmatrix} \qquad (47)$$

where

$$r_+ = \frac{r_0^+ - \mathrm{e}^{\mathrm{i}2k_+ d}}{1 - r_0^+ \mathrm{e}^{\mathrm{i}2k_+ d}} \qquad (48)$$

$$r_- = \frac{r_0^- - \mathrm{e}^{\mathrm{i}2k_- d}}{1 - r_0^- \mathrm{e}^{\mathrm{i}2k_- d}} \qquad (49)$$

and $r_0^{\pm} = \frac{Z^{\pm}-1}{Z^{\pm}+1}$, $k_{\pm} = \frac{\omega}{c_0}(\epsilon(\mu \pm \mu_g))^{\frac{1}{2}}$ and $Z^{\pm} = \left(\frac{1}{\epsilon}(\mu \pm \mu_g)\right)^{\frac{1}{2}}$.

The structure of the reflection coefficients r_+ and r_- are the same as that of the Dallenbach layer considered in Section 2. It is also seen that for the case when the waves propagate along the direction of magnetization, the material can, in terms of wave number, wave impedance and reflection coefficient, be described by an effective permeability

$$\mu_{\text{eff}}^{\pm} = \mu \pm \mu_g \tag{50}$$

It is often of interest to study the reflection for incoming waves that are linearly polarized. The reflection coefficients when the incoming wave is represented by a linearly polarized mode (instead of circularly polarized) are easily obtained from the reflection coefficients above in the following way

$$r_{\text{co}} = \frac{r_+ + r_-}{2} \tag{51}$$

$$r_{\text{cross}} = -\text{i}\frac{r_+ - r_-}{2} \tag{52}$$

where r_{co} is the reflection coefficient for the same polarization as the incoming wave and r_{cross} corresponds to the orthogonal polarization.

6. RESULTS

For the particular geometry described in Section 5, the elements of the demagnetization tensor are all zero except for N_{zz} which equals unity (see Table 2). Because of this, equations (36)–(38) become

$$\mu(\omega) = 1 + \frac{\beta - \text{i}\alpha\omega/\omega_{\text{m}}}{(\beta - \text{i}\alpha\omega/\omega_{\text{m}})^2 - (\omega/\omega_{\text{m}})^2} \tag{53}$$

$$\mu_g(\omega) = -\frac{\omega/\omega_{\text{m}}}{(\beta - \text{i}\alpha\omega/\omega_{\text{m}})^2 - (\omega/\omega_{\text{m}})^2} \tag{54}$$

$$\mu_z(\omega) = 1 \tag{55}$$

where

$$\beta = |\boldsymbol{H}_0^{\text{e}}|/M_{\text{s}} - 1 \tag{56}$$

The permittivity was set to a constant, $\epsilon = 5 + 1\text{i}$, in all of the calculations in this section. In [22, p. 715] the permittivity for different ferrite materials can be found. From this we see that our choice of

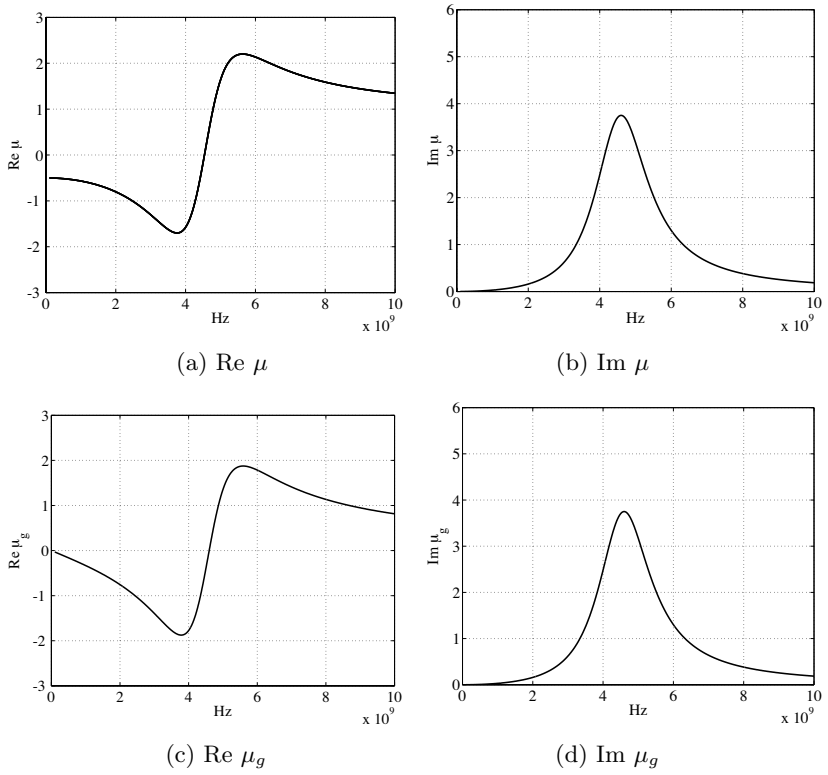

(a) Re μ (b) Im μ

(c) Re μ_g (d) Im μ_g

Figure 3. Real and imaginary parts of the permeability tensor. M_s is set to $2{\cdot}10^5$ A/m, $H_0^\mathrm{e} = M_\mathrm{s}/3$ and $\alpha = 0.2$.

permittivity is of the same order as listed even though the losses for ferrites are usually smaller.

In Figure 3, plots of the components of the permeability tensor is shown. From these it is seen that the material exhibits a resonant behavior but with finite amplitude because of the loss term in LLG equation. For small losses (*i.e.*, $\alpha \ll 1$) the resonance frequency is close to $\omega_0 = \gamma\mu_0(|\boldsymbol{H}_0^\mathrm{e}| - M_\mathrm{s})$ ($\approx 4.7\,\mathrm{GHz}$ for the parameters used in Figure 3).

Also, in Figure 4, plots of the effective permeabilities are shown. From these it is seen that the resonance behavior for μ_eff^- is absent while for μ_eff^+ the resonance peaks are increased in amplitude. This shows that there is a preferred rotation direction in terms of the circularly polarized modes. This is due to the fact that the magnetization executes a clockwise precession (viewed in the direction of the $\boldsymbol{H}_0$-field) about the $\boldsymbol{H}_0$-field at the frequency ω_0. This results in a

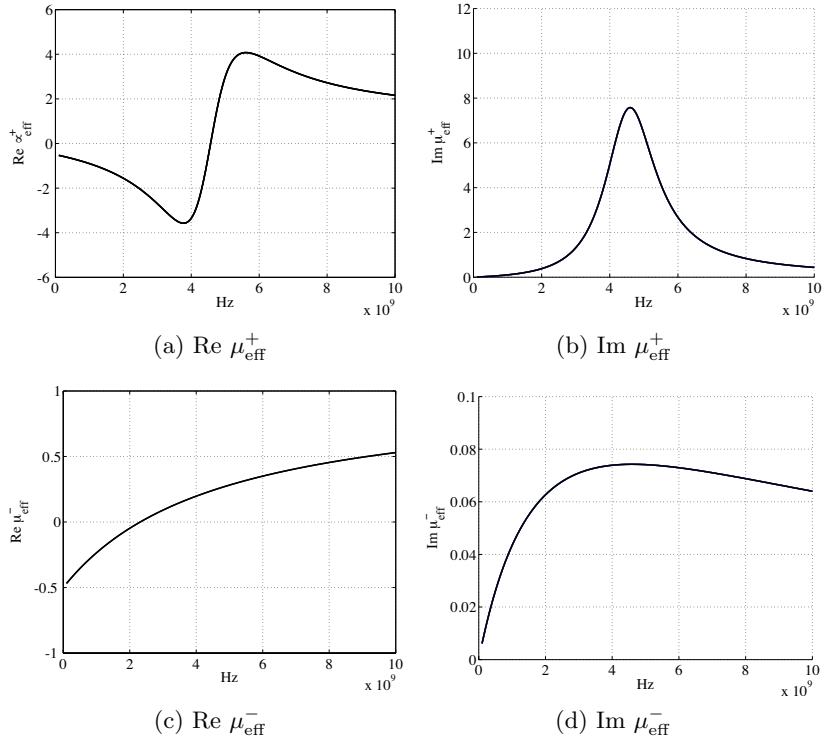

(a) Re $\mu^+_{\rm eff}$ (b) Im $\mu^+_{\rm eff}$

(c) Re $\mu^-_{\rm eff}$ (d) Im $\mu^-_{\rm eff}$

Figure 4. Real and imaginary parts of the effective permeability $\mu^{\pm}_{\rm eff} = \mu \pm \mu_g$. $M_{\rm s}$ is set to $2{\cdot}10^5$ A/m, $H^{\rm e}_0 = M_{\rm s}/3$ and $\alpha = 0.2$.

strong interaction between the mode with a circular polarization that rotates clockwise (left hand circular polarized when $M_0 > H_0$) and the medium, and induces a resonance when the two frequencies are equal, *i.e.*, when $\omega = \omega_0$. However, the circular polarized mode that rotates counter clockwise opposes the precession and thus interacts rather weakly with the medium. This is also seen from Figure 4, where the imaginary part of $\mu^-_{\rm eff}$ is much smaller than that of $\mu^+_{\rm eff}$, which means that the absorption is poorer for the mode associated with $\mu^-_{\rm eff}$.

In the limit $H^{\rm e}_0 \to M_{\rm s}$, one obtains the following expression for $\mu^{\pm}_{\rm eff}$

$$\mu^{\pm}_{\rm eff} = 1 \pm \frac{\omega_{\rm m}}{\omega(1+\alpha^2)} + {\rm i}\frac{\omega_{\rm m}\alpha}{\omega(1+\alpha^2)} \tag{57}$$

From this expression it is seen that even though it is possible

to fulfil (5), it is not possible to reach the condition (6) for a small $k_0 d$. Hence, with the LLG model one cannot expect to achieve the ideal RAM mentioned in Section 2 where we had zero reflection at all frequencies. It is also seen that in this limit, the magnitude of the imaginary part of $\mu_{\text{eff}}^{\pm}$ (and thus the losses) falls off like $\sim 1/\omega$ and depends on the damping factor α and the saturation magnetization M_{s}.

In Figures 5–10 plots of $|r_+|^2$,$|r_-|^2$, $|r_{\text{co}}|^2$ and $|r_{\text{cross}}|^2$ are shown for different strength of the biasing field. Once again it is confirmed that the mode with a circular polarization that rotates in the same direction as the precession of the magnetization has a strong interaction with the material when $\omega \approx \omega_0$. This interaction is manifested through the sharp dips in r_+ in Figures 5a,c,e. On the other hand, for the r_- mode, this resonance does not appear and the mode passes through the material without any considerable absorption. It is also seen that this resonance is shifted when the saturation magnetization is changed (or when H_0^{e} is changed), since ω_0 changes according to $\omega_0 = \gamma\mu_0(|\boldsymbol{H}_0^{\text{e}}| - M_{\text{s}})$. An additional resonance is also found to appear at approximately 30 GHz in Figures 5a,b,c,d. This resonance is associated with the thickness of the material and occurs when the thickness corresponds to roughly a quarter wavelength. This resonance occurs for slightly different frequencies for the two different modes since these two modes have different wavelengths in general. When the thickness of the material is changed one can see from Figures 5e,f that this resonance is shifted, as expected. For the special case $H_0^{\text{e}} = M_{\text{s}}$ presented in Figure 6, the resonance associated with the precession of the magnetization is no longer present since $\omega_0 = 0$ ($H_0^{\text{e}} = M_{\text{s}}$ also corresponds to $\beta = 0$, *i.e.*, the material exhibits a magnetic conductivity, see (40)). Now, only the thickness resonance remains. From (57) it is inferred that the losses will increase as M_{s} and α is increased, which then would result in a reduction of r_+ and r_-. This conclusion is also reached by studying Figures 6a,b,c,d. A noteworthy result in Figure 7 is that the resonance frequency associated with the magnetization is shifted over to the r_- mode as H_0^{e} exceeds M_{s}. This result arise from the fact that the effective H_0-field is reversed as H_0^{e} exceeds M_{s} and thus changes the precession direction of the spin. Consequently, the r_- mode now rotates in the same direction as the magnetization.

Now, analyzing the figures when the material is illuminated by a linearly polarized wave (*i.e.*, Figures 8–10), one can qualitatively understand the result in the following way: Due to the fact that r_{co} and r_{cross} is the sum and difference of r_+ and r_-, respectively, one finds that as one of the co- or cross polarization increases the other will

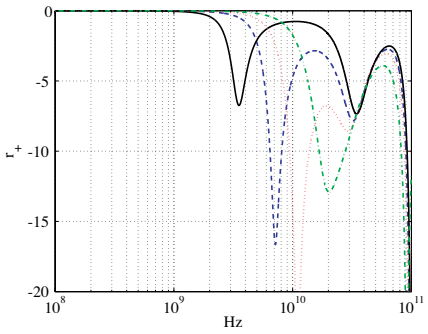

(a) M_s is swept through 1 (solid line), 2 (dashed line), 3 (dotted line) and 5 (dash-dotted line) $\cdot 10^5$A/m.

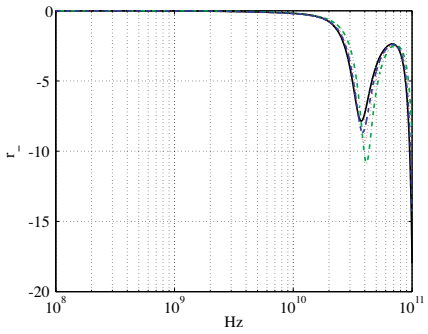

(b) M_s is swept through 1 (solid line), 2 (dashed line), 3 (dotted line) and 5 (dash-dotted line) $\cdot 10^5$A/m.

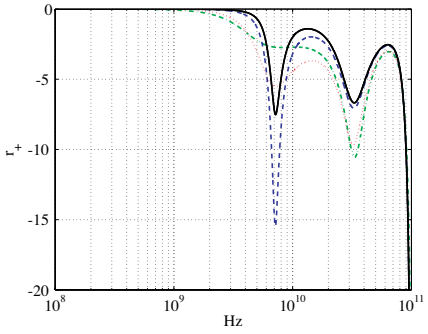

(c) α is swept through 0.05 (solid line), 0.1 (dashed line), 0.5 (dotted line) and 1 (dash-dotted line).

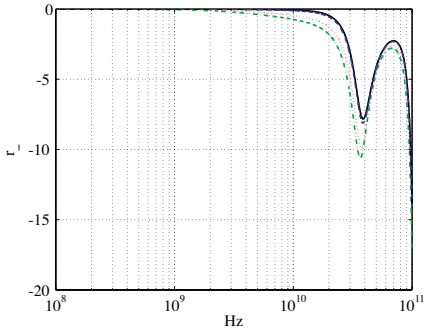

(d) α is swept through 0.05 (solid line), 0.1 (dashed line), 0.5 (dotted line) and 1 (dash-dotted line).

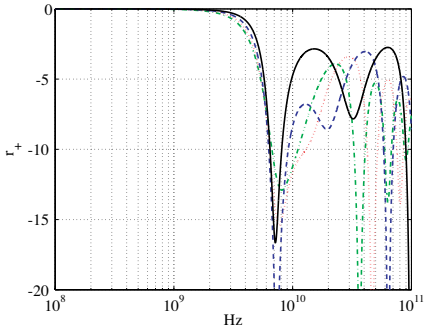

(e) d is swept through 1 (solid line), 1.5 (dashed line), 2 (dotted line) and 2.5(dash-dotted line) mm.

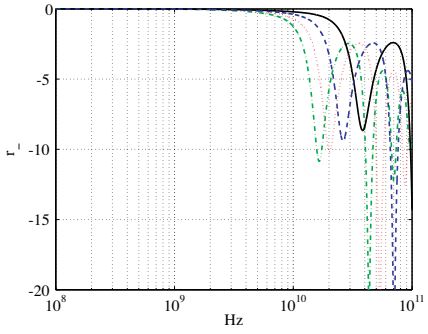

(f) d is swept through 1 (solid line), 1.5 (dashed line), 2 (dotted line) and 2.5 (dash-dotted line) mm.

Figure 5. Plots of $|r_+|^2$ and $|r_-|^2$ (in dB) for $H_0^e \ll M_s$. Default values are $M_s = 2 \cdot 10^5$ A/m , $\alpha = 0.2$, $\epsilon = 5 + 1\mathrm{i}$ and $d = 1$ mm.

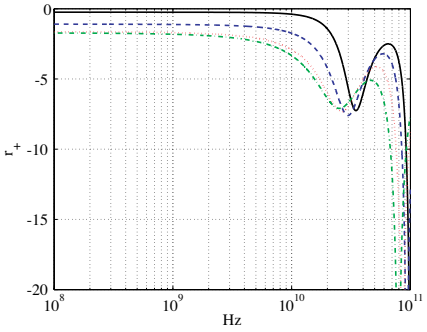

(a) M_s is swept through 1 (solid line), 5 (dashed line), 10 (dotted line) and 15 (dash-dotted line) $\cdot 10^5$A/m.

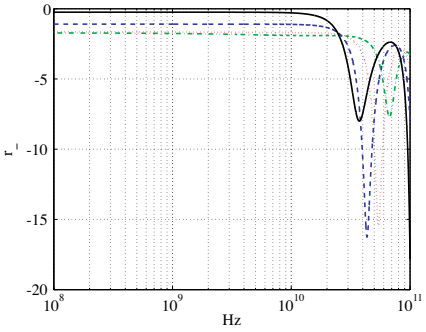

(b) M_s is swept through 1 (solid line), 5 (dashed line), 10 (dotted line) and 15 (dash-dotted line) $\cdot 10^5$A/m.

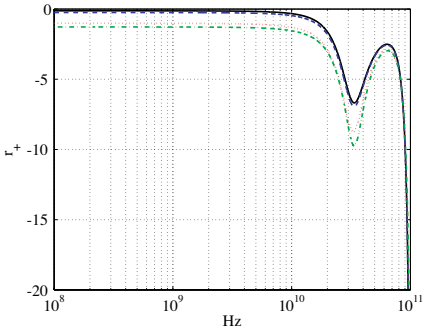

(c) α is swept through 0.05 (solid line), 0.1 (dashed line), 0.5 (dotted line) and 1 (dash-dotted line).

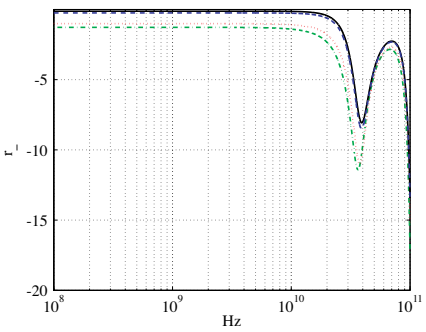

(d) α is swept through 0.05 (solid line), 0.1 (dashed line), 0.5 (dotted line) and 1 (dash-dotted line).

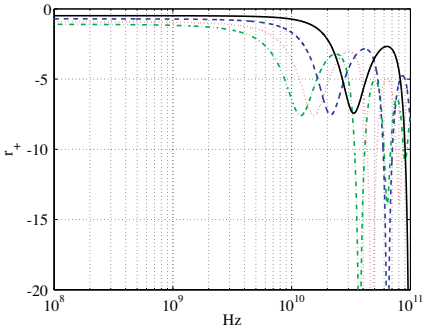

(e) d is swept through 1 (solid line), 1.5 (dashed line), 2 (dotted line) and 2.5 (dash-dotted line) mm.

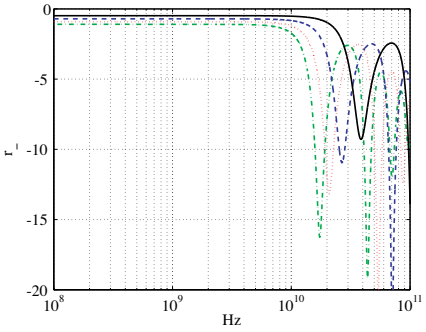

(f) d is swept through 1 (solid line), 1.5 (dashed line), 2 (dotted line) and 2.5 (dash-dotted line) mm.

Figure 6. Plots of $|r_+|^2$ and $|r_-|^2$ (in dB) for $H_0^\mathrm{e} = M_\mathrm{s}$. Default values are $M_\mathrm{s} = 2 \cdot 10^5\,\mathrm{A/m}$, $\alpha = 0.2$, $\epsilon = 5 + 1\mathrm{i}$ and $d = 1\,\mathrm{mm}$.

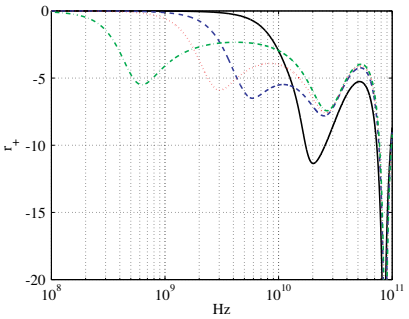

(a) H_0^e is swept through $M_s/2$ (solid line), $M_s/1.2$ (dashed line), $M_s/1.1$ (dotted line) and $M_s/1.02$ (dash-dotted line).

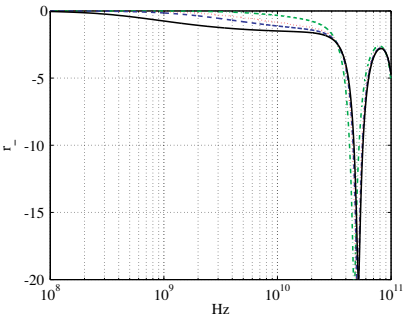

(b) H_0^e is swept through $M_s/2$ (solid line), $M_s/1.2$ (dashed line), $M_s/1.1$ (dotted line) and $M_s/1.02$ (dash-dotted line).

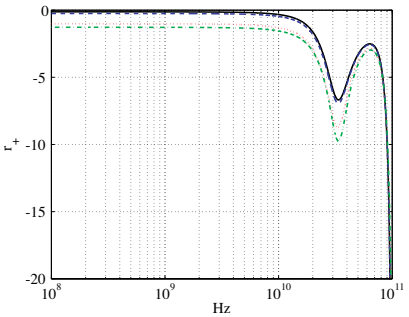

(c) H_0^e is swept through M_s (solid line), $1.02M_s$ (dashed line), $1.1M_s$ (dotted line) and $1.2M_s$ (dash-dotted line).

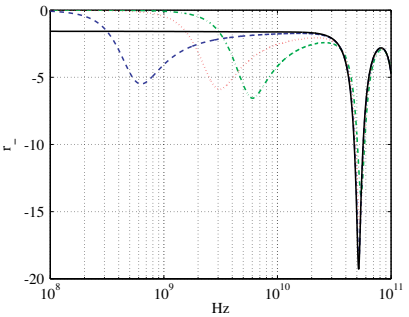

(d) H_0^e is swept through M_s (solid line), $1.02M_s$ (dashed line), $1.1M_s$ (dotted line) and $1.2M_s$ (dash-dotted line).

Figure 7. Plots of $|r_+|^2$ and $|r_-|^2$ (in dB) for different H_0^e. Default values are $M_s = 9 \cdot 10^5\,\mathrm{A/m}$, $\alpha = 0.2$, $\epsilon = 5 + 1\mathrm{i}$ and $d = 1\,\mathrm{mm}$.

decrease and this roughly means that as one gets better, the other gets worse. This behavior can also be seen from the figures. Of course, this is not always true but one also has to take the phases of r_+ and r_- into consideration in order to make a more precise analysis. For instance, it may happen that r_+ and r_- are of the same magnitude but 180 degrees out of phase, then r_{co} tend to vanish while r_{cross} becomes relatively large. Furthermore, from the figures of the reflection coefficients for the linearly polarized case, it is seen that r_{co} seems to preserve both the resonances while r_{cross} obtains local maxima at these frequencies. Also, in contrast to the eigenmodes in the material who does not couple into each other (*i.e.*, an impinging wave that is circularly polarized will not

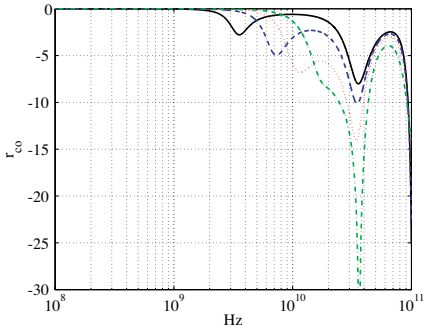

(a) M_s is swept through 1 (solid line), 2 (dashed line), 3 (dotted line) and 5 (dash-dotted line) $\cdot 10^5$A/m.

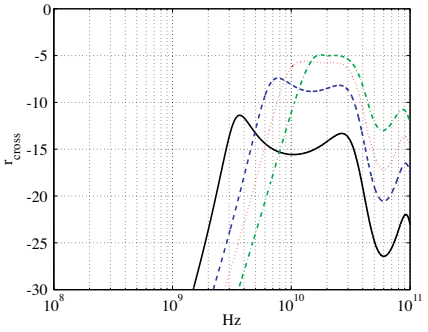

(b) M_s is swept through 1 (solid line), 2 (dashed line), 3 (dotted line) and 5 (dash-dotted line) $\cdot 10^5$A/m.

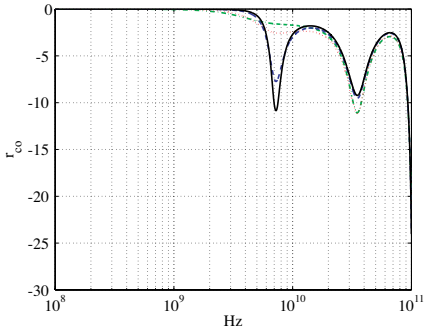

(c) α is swept through 0.05 (solid line), 0.1 (dashed line), 0.5 (dotted line) and 1 (dash-dotted line).

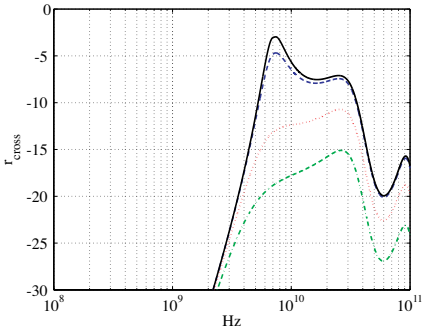

(d) α is swept through 0.05 (solid line), 0.1 (dashed line), 0.5 (dotted line) and 1 (dash-dotted line).

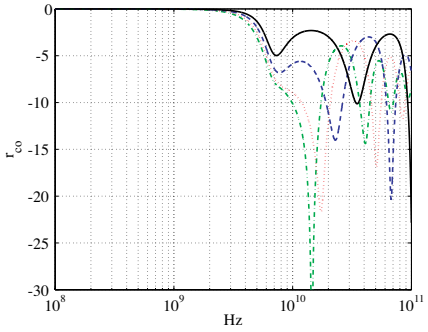

(e) d is swept through 1 (solid line), 1.5 (dashed line), 2 (dotted line) and 2.5 (dash-dotted line) mm.

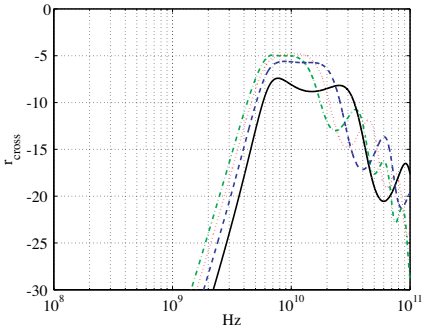

(f) d is swept through 1 (solid line), 1.5 (dashed line), 2 (dotted line) and 2.5 (dash-dotted line) mm.

Figure 8. Plots of $|r_\mathrm{co}|^2$ and $|r_\mathrm{cross}|^2$ (in dB) for $H_0^\mathrm{e} \ll M_\mathrm{s}$. Default values are $M_\mathrm{s} = 2 \cdot 10^5$ A/m , $\alpha = 0.2$, $\epsilon = 5 + 1\mathrm{i}$ and $d = 1\,\mathrm{mm}$.

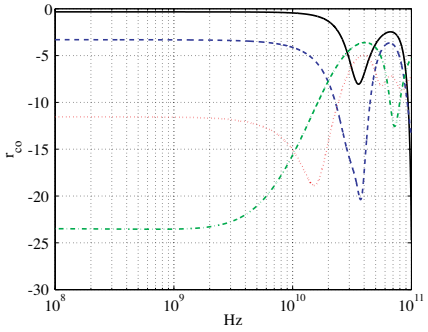

(a) M_s is swept through 1 (solid line), 5 (dashed line), 10 (dotted line) and 15 (dash-dotted line) $\cdot 10^5$A/m.

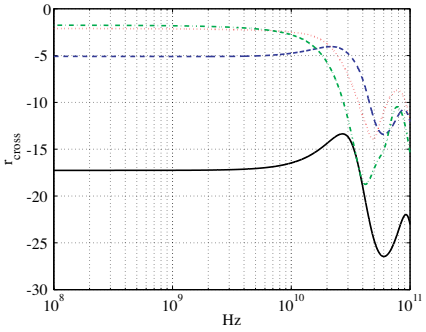

(b) M_s is swept through 1 (solid line), 5 (dashed line), 10 (dotted line) and 15 (dash-dotted line) $\cdot 10^5$A/m.

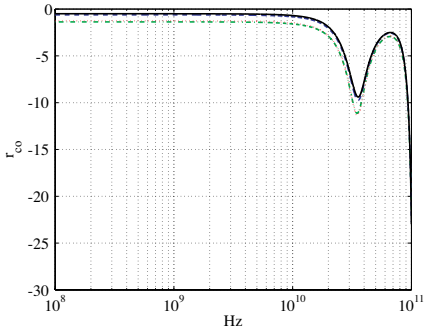

(c) α is swept through 0.05 (solid line), 0.1 (dashed line), 0.5 (dotted line) and 1 (dash-dotted line).

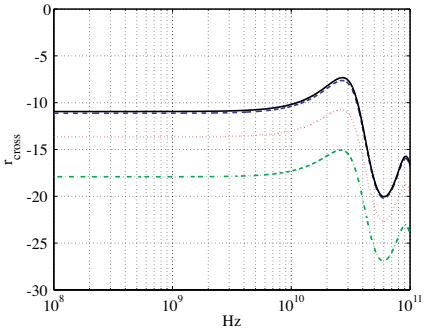

(d) α is swept through 0.05 (solid line), 0.1 (dashed line), 0.5 (dotted line) and 1(dash-dotted line).

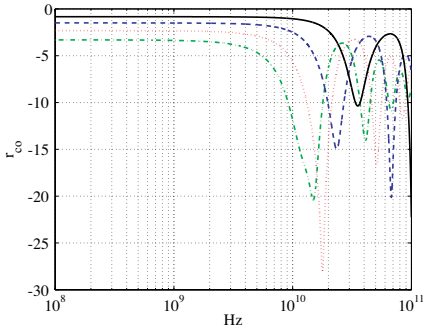

(e) d is swept through 1 (solid line), 1.5 (dashed line), 2 (dotted line) and 2.5 (dash-dotted line) mm.

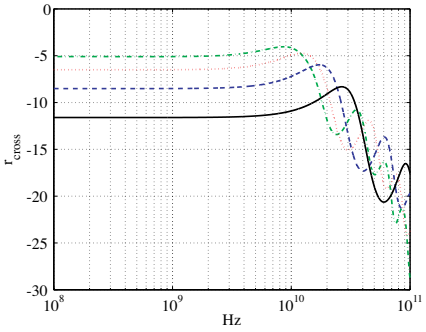

(f) d is swept through 1 (solid line), 1.5 (dashed line), 2 (dotted line) and 2.5 (dash-dotted line) mm.

Figure 9. Plots of $|r_{\mathrm{co}}|^2$ and $|r_{\mathrm{cross}}|^2$ (in dB) for $H_0^{\mathrm{e}} = M_{\mathrm{s}}$. Default values are $M_{\mathrm{s}} = 2 \cdot 10^5\,\mathrm{A/m}$, $\alpha = 0.2$, $\epsilon = 5 + 1\mathrm{i}$ and $d = 1\,\mathrm{mm}$.

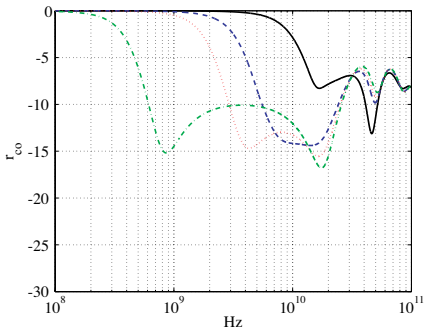

(a) H_0^e is swept through $M_s/2$ (solid line), $M_s/1.2$ (dashed line), $M_s/1.1$ (dotted line) and $M_s/1.02$ (dash-dotted line).

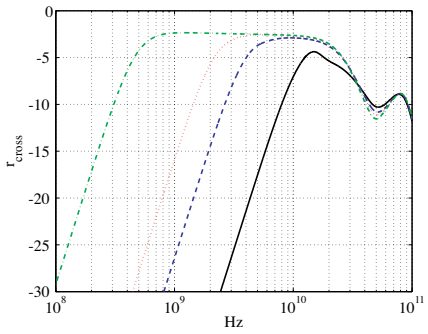

(b) H_0^e is swept through $M_s/2$ (solid line), $M_s/1.2$ (dashed line), $M_s/1.1$ (dotted line) and $M_s/1.02$ (dash-dotted line).

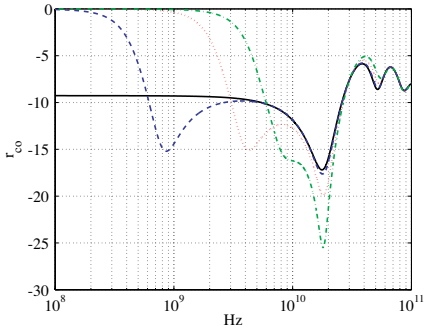

(c) H_0^e is swept through M_s (solid line), $1.02M_s$ (dashed line), $1.1M_s$ (dotted line) and $1.2M_s$ (dash-dotted line).

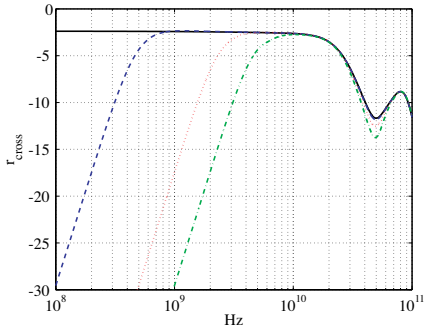

(d) H_0^e is swept through M_s (solid line), $1.02M_s$ (dashed line), $1.1M_s$ (dotted line) and $1.2M_s$ (dash-dotted line).

Figure 10. Plots of $|r_{\mathrm{co}}|^2$ and $|r_{\mathrm{cross}}|^2$ (in dB) for different H_0^e. Default values are $M_s = 9 \cdot 10^5\,\mathrm{A/m}$, $\alpha = 0.2$, $\epsilon = 5 + 1\mathrm{i}$ and $d = 1\,\mathrm{mm}$.

excited the other orthogonal polarization in the material), a linearly polarized wave will excite both polarizations. This means that if $|r_{\mathrm{co}}|^2$ or $|r_{\mathrm{cross}}|^2$ are close to unity then the other has to be close to zero since $|r_{\mathrm{co}}|^2 + |r_{\mathrm{cross}}|^2 \leq 1$ and this behavior can be verified from the figures.

7. DISCUSSION AND CONCLUSIONS

Using a linearized small signal model of the LLG equation (12), in which the material is gyrotropic and described by an effective permeability, we have shown that with the aid of a static external

biasing field, the material can be switched between a Lorentz-like material and a material that exhibits a magnetic conductivity.

Furthermore, as the material is set to behave like a Lorentz material, it was shown that by using a ferro- or ferrimagnetic layer on a PEC with a static external biasing field, one will obtain two resonance frequencies in the reflection coefficient for normally impinging waves (along the bias field) on this structure. One of these resonances is associated with the precession frequency of the magnetization and the other associated with the thickness of the layer. This is a fundamental difference between using a ferro- or ferrimagnetic layer and electric layer as absorbing material. For an electric layer, only the resonance associated with the thickness will be present. Since it is possible to shift the resonance frequency, ω_0, with the aid of the biasing field, one has the possibility to combine these two resonance frequencies that are present for magnetic materials. Hence, absorbers consisting of magnetic materials have the potential of being more broadband and thinner than electrical absorbers. However, only the eigenmode with a circular polarization that rotates in the same direction as the precession of the magnetization will experience this additional resonance whereas the other mode will experience only the resonance associated with the thickness, *i.e.*, like an electrical absorber.

For the linearly polarized case it is seen from the figures that when the bias field strength is equal or close to the saturation magnetization ($\beta \approx 0$, *i.e.*, the material exhibits a magnetic conductivity), increasing M_{s} improves r_{co} but worsen r_{cross} and increasing α improves the reflection coefficient for both polarizations. Thus, large values for M_{s} and α is needed in order to obtain a broadband absorber. More than two decades bandwidth can be achieved for a reflectivity level around $-20\,\mathrm{dB}$ at a material thickness of only 1 mm for co-polarization, see Figure 11. However, this requires a quite large value for α (0.9), and this might not be possible to obtain. The condition $\beta = 0$ may also be difficult to achieve since this requires a bias field of the order of the saturation magnetization, which is a very large field strength. Also, it is seen from the figures that the absorber is sensitive to disturbances in the bias field. Small deviations from M_{s} in the bias field results in quite different results.

At this point one should not read too much into these results in terms of bandwidths and reflectivity levels since in this analysis the electric losses are not modeled properly. For microwave ferrite materials, the electric losses are usually negligible [22, p. 715], but for ferromagnetic materials this loss is usually substantial. Even though electric losses are included they were set to be independent of frequency. The reason for this is that we wanted to isolate our

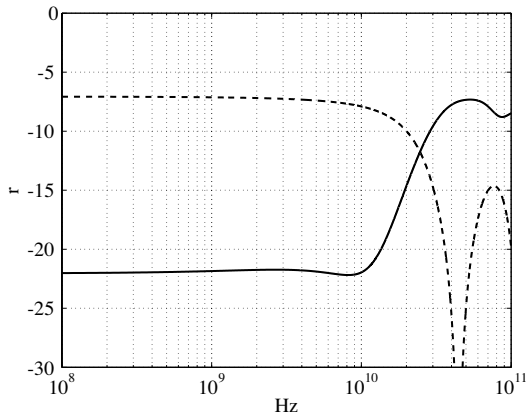

Figure 11. Plots of $|r_{\mathrm{co}}|^2$ (solid line) and $|r_{\mathrm{cross}}|^2$ (dashed(line) (in dB) for $H_0^{\mathrm{e}} = M_{\mathrm{s}}$. $M_{\mathrm{s}} = 16 \cdot 10^5$ A/m , $\alpha = 0.9$, $\epsilon = 5 + 1\mathrm{i}$ and $d = 1$ mm.

investigation to effects due to the magnetic losses and develop a better understanding of how these losses affect the absorption of electromagnetic energy. However, the ohmic losses are easily included in the analysis and then one can obtain more realistic results.

It was also discovered that the conditions for the ideal magnetic Salisbury screen (a very thin magnetic layer on a PEC with practically zero reflection at all frequencies for normally impinging waves) mentioned in Section 2 is unreachable with this model of the magnetization.

In the analysis presented here the anisotropy tensor $\mathbf{N}_{\mathrm{c}}$ was neglected. It is possible to augment the analysis to include an arbitrary anisotropy- and demagnetization tensor and obtain a closed form expression for the susceptibility tensor. However, for the case of a thin plate geometry biased in the normal direction where the material is uniaxial with its easy axis along the normal direction, it is found that this will just lead to a correction in the constant β (and hence the resonance frequency) of the form $\beta = |\boldsymbol{H}_0^{\mathrm{e}}|/M_{\mathrm{s}} - 1 - N_{\mathrm{c}}$. Hence, it does not change the fundamental physics of the problem for this particular case. Therefore we have chosen not to include the full analysis containing an arbitrary anisotropy tensor.

REFERENCES

1. Knott, E. F., J. F. Shaeffer, and M. T. Tuley, *Radar Cross Section*. SciTech Publishing Inc., 2004.
2. Gustafsson, M., "RCS reduction of integrated antenna arrays with resistive sheets," *J. Electro. Waves Applic.*, Vol. 20, No. 1, 27–40, TEAT-7135, 2006.
3. Gustafsson, M., "Surface integrated dipole arrays with tapered resistive edge sheets," *J. Electro. Waves Applic.*, Vol. 21, No. 6, 713–718, 2007.
4. Ruck, G. T., D. E. Barrick, W. D. Stuart, and C. K. Krichbaum, *Radar Cross Section Handbook*, Vol. 2, Plenum Press, 1970.
5. Sjöberg, D., "On uniqueness and continuity for the quasi-linear, bianisotropic Maxwell equations, using an entropy condition," *Progress In Electromagnetics Research*, PIER 71, 317–339, 2007.
6. Strifors, H. C. and G. C. Gaunaurd, "Bistatic scattering by bare and coated perfectly conducting targets of simple shape," *J. of Electromagn. Waves and Appl.*, Vol. 20, No. 8, 1037–1050, 2006.
7. Gong, Z. Q. and G. Q. Zhu, "FDTD analysis of an anisotropically coated missile," *Progress In Electromagnetics Research*, PIER 64, 69–80, 2006.
8. Musal, J. H. M. and H. T. Hahn, "Thin-layer electromagnetic absorber design," *IEEE Trans. Magnetics*, Vol. 25, 3851–3853, Sept. 1989.
9. Kim, S. S. and D. Han, "Microwave absorbing properties of sintered $Ni - Zn$ ferrite," *IEEE Trans. Magnetics*, Vol. 30, No. 6, 4554–4556, 1994.
10. Shin, J. Y. and J. H. Oh, "The microwave absorbing phenomena of ferrite microwave absorbers," *IEEE Trans. Magnetics*, Vol. 29, No. 6, 3437–3439, 1993.
11. Cho, H. S. and S. S. Kim, "M-hexaferrites with planar magnetic anisotropy and their application to high-frequency microwave absorbers," *IEEE Trans. Magnetics*, Vol. 35, No. 5, 3151–3253, 1999.
12. Pinho, M. S., M. L. Gregori, R. C. R. Nunes, and B. G. Soares, "Performance of radar absorbing materials by waveguide measurements for X- and Ku-band frequencies," *European Polymer Journal*, Vol. 38, 2321–2327, 2002.
13. Haijun, Z., L. Zhichao, M. Chengliang, Y. Xi, Z. Liangying, and W. Mingzhong, "Complex permittivity, permeability, and microwave absorption of Zn- and Ti-substituted barium ferrite

by citrate sol/gel process," *Materials Science and Engineering B*, Vol. 96, 289–295, 2002.

14. Meshrama, M., N. K. Agrawal, B. Sinha, and P. Misra, "Characterization of M-type barium hexagonal ferrite-based wide band microwave absorber," *Journal of Magnetism and Magnetic Materials*, Vol. 271, 207–214, 2004.
15. Kim, S.-S., S.-T. Kim, J.-M. Ahn, and K.-H. Kim, "Magnetic and microwave absorbing properties of Co-Fe thin films plated on hollow ceramic microspheres of low density," *Journal of Magnetism and Magnetic Materials*, Vol. 271, 39–45, 2004.
16. Zhang, B., G. Lu, Y. Fenga, J. Xiong, and H. Lu, "Electromagnetic and microwave absorption properties of Alnico powder composites," *Journal of Magnetism and Magnetic Materials*, Vol. 299, 205–210, 2006.
17. Engström, C. and D. Sjöberg, "On two numerical methods for homogenization of Maxwell's equations," *Journal of Electromagnetic Waves and Applications*, Vol. 21, No. 13, 1845–1856, 2007.
18. Wallace, J. L., "Broadband magnetic microwave absorbers: Fundamental limitations," *IEEE Trans. Magnetics*, Vol. 29, No. 6, 4209–4214, 1993.
19. Bregar, V. B., "Advantages of ferromagnetic nanoparticle composites in microwave absorbers," *IEEE Trans. Magnetics*, Vol. 40, No. 3, 1679–1684, 2004.
20. Wu, L. Z., J. Ding, H. B. Jiang, L. F. Chen, and C. K. Ong, "Particle size influence to the microwave properties of iron based magnetic particulate composites," *Journal of Magnetism and Magnetic Materials*, Vol. 285, 233–239, 2005.
21. Collin, R. E., *Foundations for Microwave Engineering*, 2nd edition, McGraw-Hill, 1992.
22. Pozar, D. M., *Microwave Engineering*, Addison-Wesley, 1990.
23. Kong, J. A., *Theory of Electromagnetic Waves*, John Wiley & Sons, 1975.
24. Jackson, J. D., *Classical Electrodynamics*, 3rd edition, John Wiley & Sons, 1998.
25. Kittel, C., *Introduction to Solid State Physics*, 7th edition, Wiley & Sons, 1996.
26. Kittel, C., "Physical theory of ferromagnetic domains," *Rev. Mod. Phys.*, Vol. 21, 541–583, Oct. 1949.
27. Goodenough, J. B., "Summary of losses in magnetic materials," *IEEE Trans. Magnetics*, Vol. 38, 3398–3408, Sept. 2002.

28. Elliot, R. S., *An Introduction to Guided Waves and Microwave Circuits*, Prentice Hall, 1993.
29. Sodha, M. S. and N. C. Srivastava, *Microwave Propagation in Ferrimagnetics*, Plenum Press, 1981.
30. Landau, L. D. and E. M. Lifshitz, "On the theory of the dispersion of magnetic permeability in ferromagnetic bodies," *Physik. Z. Sowjetunion*, Vol. 8, 153–169, 1935.
31. Gilbert, T. L., "A phenomenological theory of damping in ferromagnetic materials," *IEEE Trans. Magnetics*, Vol. 50, 3443–3449, Nov. 2004.
32. Yu, Y. and J. W. Harrel, "FMR spectra of oriented γ-Fe_2O_3, Co-γ-Fe_20_3, CrO_2, and MP tapes," *IEEE Trans. Magnetics*, Vol. 30, No. 6, 4083–4085, 1994.
33. Kikuchi, R., "On the minimum of magnetization reversal time," *J. Appl Phys.*, Vol. 27, 1352–1357, Nov. 1956.
34. Mallison, J. C., "On damped gyromagnetic precession," *IEEE Trans. Magnetics*, Vol. 23, 2003–2004, July 1987.
35. Barybin, A. A., "Excitation theory for space-dispersive active media waveguides," *J. Phys. D: Applied Phys.*, Vol. 32, 2014–2028, June 1999.
36. d'Aquino, M., "Nonlinear magnetization dynamics in thin-films and nanoparticles," Ph.D. thesis, Universita degli studi di Napoli "Federico II", Facolta di Ingegneria, Napoli, Italy, 2004.
37. Yaghjian, A. D., "Electric dyadic green's functions in the source region," *Proc. IEEE*, Vol. 68, No. 2, 248–263, 1980.
38. Barybin, A. A., "Modal expansions and orthogonal complements in the theory of complex media waveguide excitation by external sources for isotropic, anisotropic, and bianisotropic media," *Progress In Electromagnetics Research*, PIER 19, 241–300, 1998.